Sinusoidal Clock Sampling for Multigigahertz ADCs

Rui Bai, Jingguang Wang, Lingli Xia, Feng Zhang, Zongren Yang, Weiwu Hu, and Patrick Chiang, *Member, IEEE*

Abstract—Current multigigahertz ADC performance is limited by the sampling clock timing jitter. This paper describes the effects of clock transition time on the spurious-free dynamic range (SFDR) of a CMOS T/H circuit. A signal-dependent nonlinearity model is first introduced that provides insight on the effect of finite clock transition time, and presents the use of sinusoidal signal as the sampling clock to improve SFDR. Whereas a square-wave clock exhibits a shorter transition time but more jitter susceptibility, sinusoidal clocking provides a longer transition time but a lower jitter spectrum. To verify this concept, an 8 GS/s, 4b flash ADC with a sinusoidal clock is designed and experimentally measured, achieving a figure-of-merit of 0.86 pJ/conv-step based upon effective resolution bandwidth (ERBW), and 0.2 pJ/conv-step based upon sampling rate.

Index Terms—Flash ADC, jitter, SFDR, sinusoidal clock.

I. INTRODUCTION

HIGH-SPEED analog-to-digital converters (ADC) are used in many communication and signal processing applications, such as UWB systems [1], SerDes receivers[2], and optical communication systems [3]. For an ADC with a sampling rate above GS/s, a high-speed track-and-hold (T/H) circuit is typically used in the front-end, followed by time-interleaving sub-ADCs [2]–[9]. In order to meet the stringent performance requirements of such ADCs (multi-gigahertz sampling rate, 5–8 bits resolution), the T/H circuit requires high linearity and wide bandwidth. Furthermore, the performance of the ADC is usually limited by the jitter of the sampling clock [7]–[9]. Even a small sampling uncertainty can introduce a large error in the sampled voltage, resulting in harmonic distortion at the output. If other nonidealities are ignored, with a sinusoidal input, the
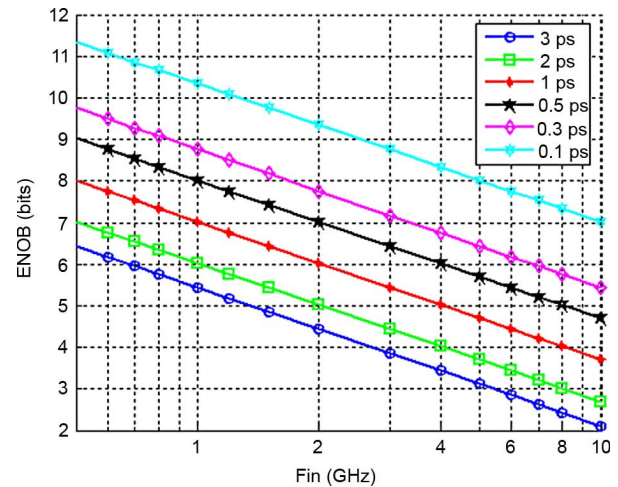
R. Bai, L. Xia, and P. Chiang are with the Electrical Engineering Computer Science Department, Oregon State University, Corvallis, OR 97331 USA (e-mail: bai@eecs.oregonstate.edu; pchiang@eecs.oregonstate.edu).

J. Wang was with the Electrical Engineering Computer Science Department, Oregon State University. He is now with the Broadcom Corporation, Irvine, CA 92617 USA (e-mail: jgwang@broadcom.com).

F. Zhang was with the Institute of Computing Technology, Chinese Academy of Sciences. He is now with the Institute of Microelectronics, Chinese Academy of Sciences (e-mail: zhangfeng_ime@ime.ac.cn).

Z. Yang and W. Hu are with the Institute of Computing Technology, Chinese Academy of Sciences, Beijing, China (e-mail: hww@ict.ac.cn).

Color versions of one or more of the figures in this paper are available online at http://ieeexplore.ieee.org.

Digital Object Identifier 10.1109/TCSI.2011.2157742

Fig. 1. ENOB versus signal frequency with varying RMS clock jitter values.

signal-to-noise ratio (SNR), due to a sampling clock with RMS jitter $\varepsilon_{\mathrm{rms}}$, is given by [4], [10]

$$\mathrm{SNR} = -20\log(2\pi \cdot f_{in}\varepsilon_{s}) \text{ dB} \qquad (1)$$

where f_{in} is the input sinusoidal signal frequency. The effective number of bits (ENOB) of the ADC versus input signal frequency with different RMS jitter values is plotted in Fig. 1. For example, in order to build an ADC with 2 GHz signal bandwidth and 6-bit resolution, the clock jitter must be less than 1 ps.

Typically, a short transition time square-wave signal is usually used as the sampling clock, generated by a chain of inverter buffers. The problem with these clock buffers is that they are susceptible to supply noise [11], especially when the ADC needs to share supply grid and substrate with noisy digital blocks on the same die.

Alternatively, if a low-jitter sinusoidal clock is generated locally to directly drive (or through a single stage of current-mode logic (CML) buffering) the T/H circuit in the ADC, the sampling uncertainty will be reduced. For example, a sinusoidal clock generated by an on-chip LC-VCO is the lowest jitter, multigigahertz source in a standard CMOS process. Unfortunately, compared with square-wave clock, the sinusoidal clock exhibits a slow slew rate during the clock transition, introducing an input signal dependent sampling error. This sampling error may then cause further distortion in the high-speed T/H circuit [12].

In Section II of this paper, the signal-dependent sampling error resulting from finite clock transition time will be analyzed mathematically, followed by a comparison between the calculated and simulated results. Then the simulated SFDR of a realistic, high-speed NMOS T/H circuit with varying amounts of
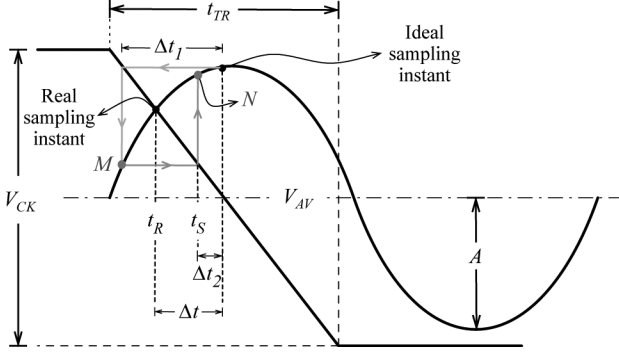
Fig. 2.   Nonlinearity model for an input-dependent sampling instant.

sampling clock transition time is presented, where the effects of signal-dependent nonlinearity on the SFDR are discussed. Section III presents the performance of this T/H circuit with a sinusoidal sampling clock. Sections IV and V then introduce a new architecture of multigigahertz ADCs using sine-wave sampling, based on the above analyses. Section VI draws the conclusion.

II. SIGNAL-DEPENDENT SAMPLING ERROR

Consider a NMOS T/H switch with its gate controlled by the clock, and source (or drain) connected to the input. When V_{gs} is larger than the V_{th} of the NMOS switch, the switch turns on and the output will track the input signal; otherwise the switch is turned off and the output holds the sampled signal. Fig. 2 shows the clock transitioning downwards, and its sampling position in the time domain. For the purpose of simplicity, the V_{th} is assumed to be zero, such that the switch is turned off when the clock signal is lower than the input signal. If there is no input signal dependency, the sampling point will always occur when the clock reaches V_{AV}, annotated by t_S in Fig. 2. However, in reality, the sampling instant takes place at t_R because that is the time when the clock voltage is the same as the input signal. Therefore for different input signal voltages, the sampling point will be different, resulting in signal level-dependent sampling error [10], [12].

A. Nonlinearity Model for Input-Dependent Sampling

Because of the input-dependent Δt change at each sampling instance, the output of the T/H is

$$V_{\text{out}}(t_S) = A \sin \omega (t_S - \Delta t) \tag{2}$$

where Δt is equal to $t_S - t_R$ as shown in Fig. 2. The crossing point between the input sine-wave and the clock falling edge is found from the solution to the following equations:

$$\begin{cases} y = A \sin \omega t \\ y = \frac{V_{CK}}{t_{TR}} (t - t_s). \end{cases} \tag{3}$$

Here we assume the input sine-wave exhibits a swing of A and frequency of ω, the square-wave clock amplitude is V_{CK}, and the transition time is t_{TR}. In order to calculate Δt, we need to find the expression of t in term of t_S. Unfortunately, there is no

mathematical solution for (3). Therefore we use an approximation method to find an estimation of Δt.

First, the sinusoidal value at time t_S is defined as $A \sin(\omega t_S)$. By putting this same value to the line expression of the clock falling edge, we can calculate Δt_1 as shown in Fig. 2, where the time difference for the sampling clock and sampled signal to reach $A \sin(\omega t_S)$ is:

$$\Delta t_1 = \frac{A \sin(\omega \cdot t_S) \cdot t_{TR}}{V_{CK}} \tag{4}$$

Δt_1 is a good estimation of Δt, but we can bring this estimation even closer. From (2) and (4), we can obtain that the sinusoidal curve expression at point M is

$$V_M(t_S) = A \sin \omega \cdot \left(t - \frac{A \sin(\omega \cdot t_S) \cdot t_{TR}}{V_{CK}} \right). \tag{5}$$

Similar to what was used to calculate Δt_1, if V_M is substituted into the line expression for a falling clock edge, we can calculate Δt_2 as shown in Fig. 2

$$\Delta t_2 = \frac{V_M(t_S) \cdot t_{TR}}{V_{CK}}. \tag{6}$$

With this value of Δt_2 we can obtain an expression for the value of point N on a sinusoidal curve

$$V_N(t_S)$$
$$= A \sin \omega \cdot \left[t_S - \frac{A \sin \omega \cdot \left(t_S - \frac{A \sin(\omega \cdot t_S) \cdot t_{TR}}{V_{CK}} \right) \cdot t_{TR}}{V_{CK}} \right]. \tag{7}$$

By carrying out this search recursively, a better estimation of the actual sampling point can be reached. Because N is already close enough to calculate the third order harmonic, the Taylor series expansion on the right side of (7) gives

$$V_N(t_S) = \left(A + \frac{17}{8} \frac{A^3 \omega^2 t_{TR}^2}{V_{CK}^2} \right) \sin \omega t_S$$
$$- \frac{3}{8} \frac{A^3 \omega^2 t_{TR}^2}{V_{CK}^2} \sin t_S + \cdots \tag{8}$$

The third-order harmonic is usually the dominant distortion component for a differential input, so for a T/H circuit with input-dependent sampling error, the SFDR can be estimated as

$$\text{SFDR} = \frac{A + \frac{17}{8} \frac{A^3 \cdot \omega^2 \cdot t_{TR}^2}{V_{CK}^2}}{\frac{3}{8} \frac{A^3 \cdot \omega^2 \cdot t_{TR}^2}{V_{CK}^2}} \approx \frac{8 \cdot V_{CK}^2}{3 \cdot A^2 \cdot \omega^2 \cdot t_{TR}^2}. \tag{9}$$

Observe that the SFDR is proportional to the square of the clock amplitude V_{CK}, inversely proportional to the square of the clock transition time t_{TR}, input signal swing A, and input signal frequency ω.

B. Calculated Result Versus Simulated Result

In order to verify the nonlinearity model derived above, we use an ideal switch where only the signal dependent sampling nonlinearity is considered.
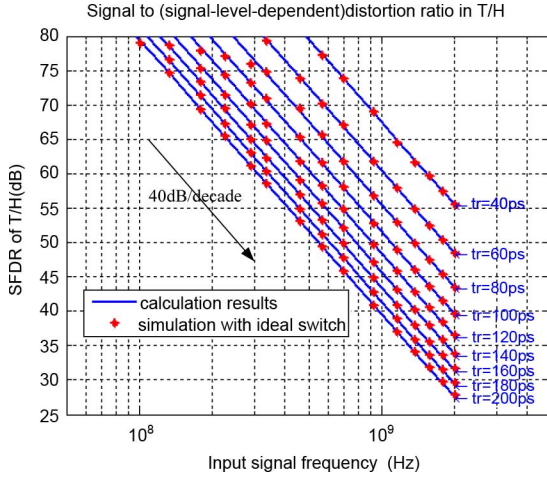
Fig. 3. SFDR limited by signal-dependent sampling error, with calculated and simulated results (clock amplitude 1.5 Vp-p, input signal swing 0.8 Vp-p).
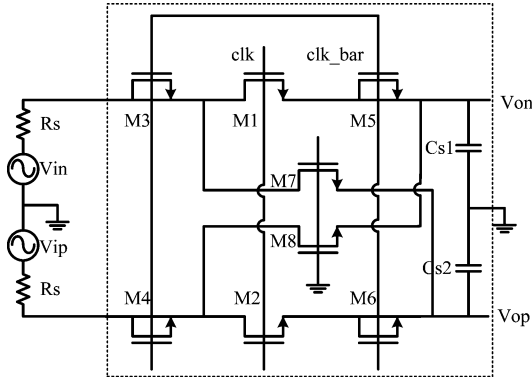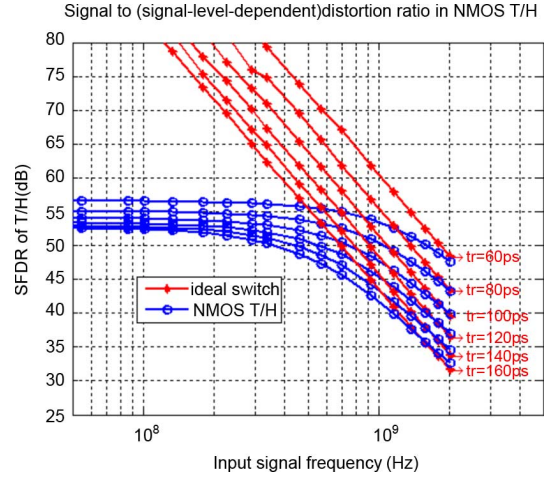

Fig. 5. SFDR simulations of an ideal switch versus NMOS T/H switch across varying clock rise time.

size of M1/M2. M7 and M8 are introduced to provide signal feed-through compensation in hold mode. In this T/H simulation, the clock and input signals are characterized similar to the preceding ideal switch simulation.

Fig. 5 shows the simulation results comparing the NMOS T/H circuit with the ideal switch T/H circuit. Considering only the signal-dependent sampling error, we can observe the following:

- At low frequency ($f_{in} < 500$ MHz), the signal dependent sampling error is not significant compared to other nonlinearity effects, but it dominates at higher frequency because it increases by 40 dB/decade.
- Other nonlinearity issues like switch turn-on resistance modulation is also dependent on clock transition time. For example, at low frequency, the SFDR with a 60 ps clock transition time is about 4 dB higher than that with a 160 ps clock transition time. In other words, clock transition time only slightly affects those nonlinearities.
- Although the signal-dependent sampling nonlinearity dominates at high frequency, with reasonable clock transition time and input signal swing, the introduced distortion can still be smaller than that caused by increased clock jitter.

III. SINUSOIDAL CLOCK SAMPLING T/H CIRCUITS

In Fig. 5, the SFDRs of the T/H circuit with varying clock transition times are compared. If a sinusoidal signal is used as the sampling clock instead, the slew rate of the clock is

$$SR = \frac{\mathrm{d}(A \sin \omega t)}{dt} = A\omega \cos(\omega t). \qquad (10)$$

The slew rate (SR) is proportional to the clock frequency, and a maximum slew rate occurs when $\omega t = n\pi$, $(n = 0, \pm 1, 2 \cdots)$. For multigigahertz clocks, the slew rate of a sine-wave clock is comparable to that of a square-wave clock, which is limited by the loading capacitance and the buffer current in real implementation. For example, a 4 GHz sine-wave clock has almost the same slew rate as a square-wave clock with 80 ps transition time and the same voltage swing.

Fig. 6 shows the SFDR of the T/H circuit with a sine-wave clock and a square-wave clock. At high frequency, the SFDR of
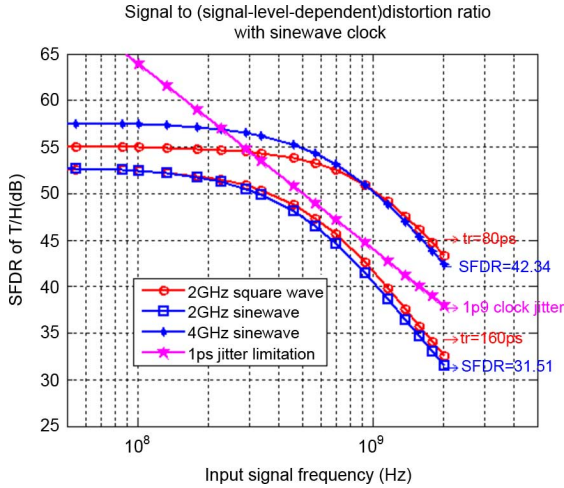

Fig. 4. Schematic of a differential NMOS T/H circuit.

Fig. 3 shows the derived and simulated results for different clock transition times and input signal frequencies. With the same clock and signal amplitude, the model matches the simulation results very well, as the SFDR rolls off by 40 dB/decade as expected when the input signal frequency increases. Note that the third harmonic distortion deteriorates by about 12 dB as the clock transition time doubles. For a wideband ADC, the sampling clock with a long transition time will limit the resolution. For example, if the clock transition time is 120 ps and the input signal frequency is 2 GHz, the signal-dependent sampling error limits the SFDR to approximately 36.5 dB.

C. SFDR Limitation in T/H Circuits

Besides the signal-dependent sampling nonlinearity, a real T/H circuit exhibits distortions and noise from other sources such as charge injection, switch turn-on resistance modulation, and clock feed-through, further deteriorating the SFDR. In order to find out the dominant nonideality within a high-speed T/H, as well as determine the minimum requirement of the clock transition time for a multigigahertz ADC (i.e., 6-bit 2 GHz signal bandwidth ADC), a differential NMOS T/H circuit is designed within a 90 nm CMOS process, as shown in Fig. 4.

M1 and M2 are the differential sampling switches driven by clk. The dummy transistors M3-M6, controlled by clk_bar, are used to reduce the charge injection when M1/M2 switch from track mode to hold mode [13]. M3-M6 are half the

Fig. 6. SFDR of NMOS T/H circuits with both sine-wave and square-wave clocking (input signal swing 0.8 Vp-p, clock swing 1.5 Vp-p).

Fig. 7. Architecture of proposed Flash ADC.

the 4 GHz sine-wave clock is close to that of the 80 ps transition time square-wave clock. This is expected because they have comparable slew rates. In Fig. 6, we also plot the SNR limit in a T/H circuit when 1 ps RMS jitter is present in the sampling clock. As observed, for a 6-bit 2 GHz bandwidth ADC, the clock jitter should be smaller than 1 ps. Since the ADC is typically used in a system-on-a-chip with noisy digital blocks, it may be nontrivial to generate a square-wave clock with such small jitter, and a low-noise clock buffer can also be power hungry. Instead, if a 4 GHz sine-wave is used as the sampling clock, a lower clock jitter can be utilized at the expense of a larger input-dependent sampling error. As shown in Fig. 6, using a 4 GHz sine-wave sampling clock limits the SFDR to approximately 42 dB for a 2 GHz input bandwidth. This is still 6 dB higher than the SNDR required for a 6-bit ADC.

IV. DESIGN EXAMPLE: FLASH ADC INCORPORATING SINE-WAVE SAMPLING

Based on our previous analysis on the advantages of sine-wave sampling, an 8 Gs/s flash ADC is proposed that incorporates a sine-wave clock source. Fig. 7 shows the overall schematic of the ADC. The input data is directly sampled by 15 comparators, each followed by a SR-latch to generate a 15b thermometer code. To reduce the probability of errors caused by comparator metastability, a bubble correction stage is used. Finally a 4-bit Gray code is generated by the ROM-based decoder.

The sine-wave clock source can be generated using an on-chip LC-VCO, which either directly drives the capacitance loading of the comparators through resonant clocking [11], or using a single-stage CML buffer that separates the LC-VCO from possible noise kickback. Using a resistively loaded CML buffer adds to power consumption, as large static current is needed to achieve near full-rail clock swing. Alternatively, an injection-locked VCO can be used as a clock buffer to drive the entire load capacitance. However, accurate control of the actual resonant clock frequency due to the presence of parasitic
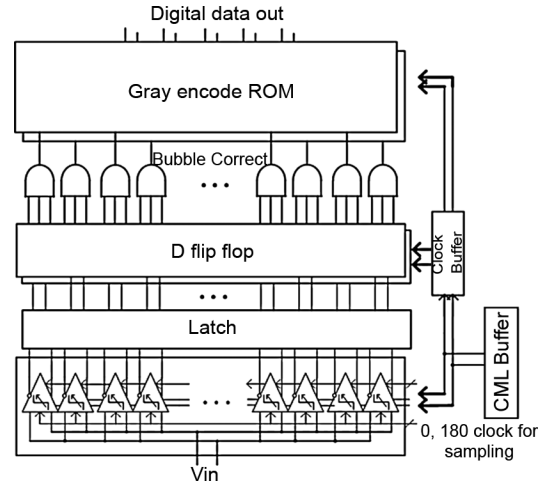
loading of the large wiring/gate capacitance is difficult in practice [11].

Fig. 8 shows the schematic of the comparator used in the ADC. Current steering is shared between two comparators working in bang-bang mode at 4 GHz, realizing an effective sampling rate of 8 GS/s. Each comparator is folded into two stages in order to operate under a low supply [6].

The first stage works as both a sampler and a preamplifier. It is followed by the latch stage. The PMOS load in the first stage is turned off in sampling mode in order to achieve a higher sampling bandwidth. After the comparator has completed sampling, the PMOS load turns on to reset the latch. Another advantage of this comparator is that clock kickback is eliminated because the switches are connected to the common mode point in the signal path.

Fig. 9 here shows the simulated results of comparator quantization delay for different input amplitudes, for both a 4 GHz sine-wave clock and a 20 ps rise-time square wave clock. The difference in quantizer delay is less than 5 ps for all input signals. This delay degradation is minimized due to the current steering nature of the complementary quantizers, where absolute clock voltage is less important than the ability for the differential pair to hard switch the current from one branch to the other.

In deep submicrometer CMOS processes, the mismatch and process variation is a critical limitation. Monte-Carlo analysis indicates that 3-sigma variation introduces about ± 40 mV of input-referred offset in our design. In this design, a digitally controlled 6-bit current source provides extra current for the output nodes of the first stage in order to introduce an intentional offset and hence, process variation calibration [14].

One possible concern is whether the sinusoidal clock exhibits a fast-enough sampling bandwidth, compared to the conventional, square-wave clock. We simulate the pulse sensitivity function to evaluate the sampling bandwidth of the comparator. As shown in Fig. 10, only a 0.2 dB difference exists in the transfer function at 4 GHz when sampled by either the sinusoidal clock or 20 ps rise/fall time clock. Therefore,
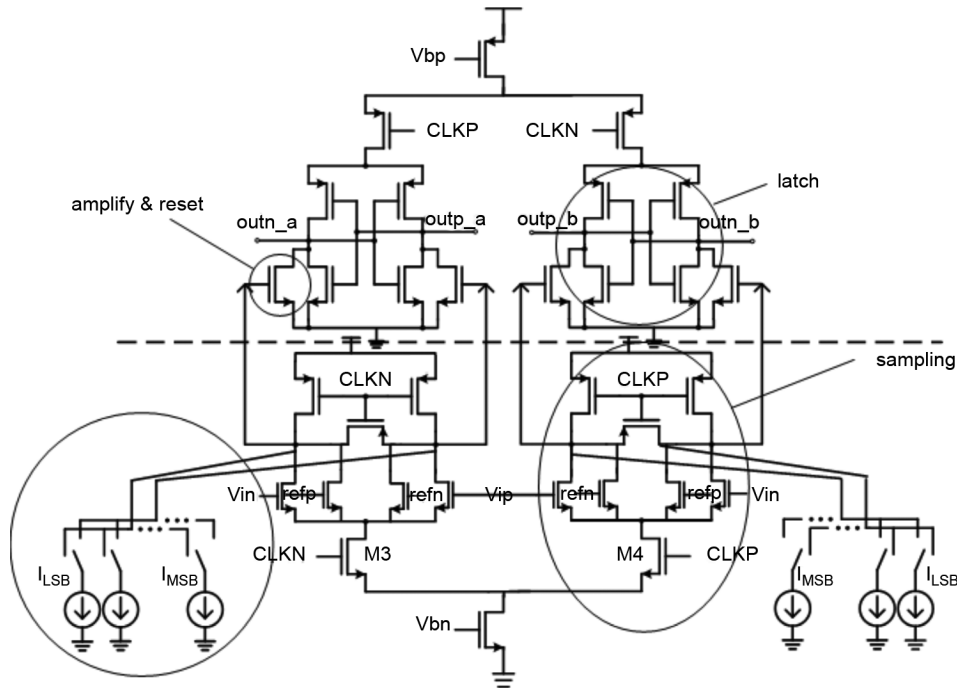
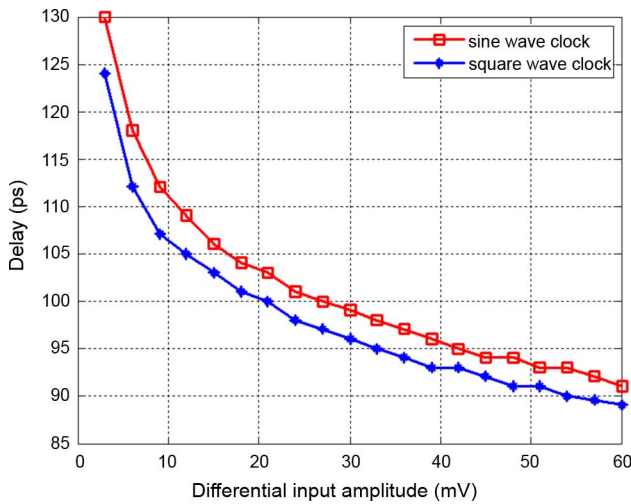Fig. 8.   Schematic of comparator with offset calibration.

Fig. 9.   Comparator delay with various input amplitude.

Fig. 10.   Comparator sampling bandwidth, comparing a sine-wave with square wave clocking.

a sinusoidal sampling clock does not significantly affect the performance of this ADC up to the Nyquist bandwidth.

V. EXPERIMENTAL MEASUREMENTS

The ADC was fabricated in a standard 65 nm CMOS technology.Fig. 11 shows the micrograph of the ADC. The ADC was wire-bonded using chip-on-board to a PCB. While great care was taken initially to maintain a large input bandwidth, several problems manifested during the measurement testing, resulting in severely degraded performance. First, ESD devices were not incorporated into the original design in order to improve bandwidth. Unfortunately, the thin oxide of this 65 nm-CMOS process is severely sensitive to ESD, preventing reliable measurements. Hence, off-chip ESD packages of size 2.7 pF had to be incorporated into a second board revision, loading the input impedance. Second, a wideband balun was designed
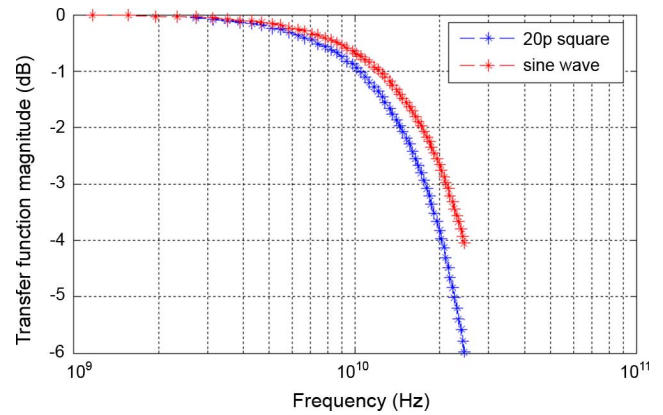
to enable single-ended to differential conversion from the off-chip sinusoidal signal generator. Unfortunately, the balun low-pass filtered input frequencies below 1 MHz (such as a slow linear ramp), preventing calibration and cancellation of dc offsets in the comparators. Hence, the balun was eliminated and a 1 cm shorting wire was employed to connect the input traces. Finally, small ac coupling capacitors were utilized in the signal chain in order to independently set the input common-mode, also degrading input bandwidth.

All of these nonideal discontinuities result in significant distortion in the step response for the PCB differential input. Shown in Fig. 13 above is the step response at various places on the PCB after performing a time-domain reflectometer (TDR). Here, the final signal bandwidth at the input to the chip, after wave propagation through these multiple discontinuities, shows a rise time and estimated input bandwidth of less than 1 GHz.

The prototype operates with a 1 V analog and 1.2 V digital supply voltage. The output of the ADC is decimated by 64
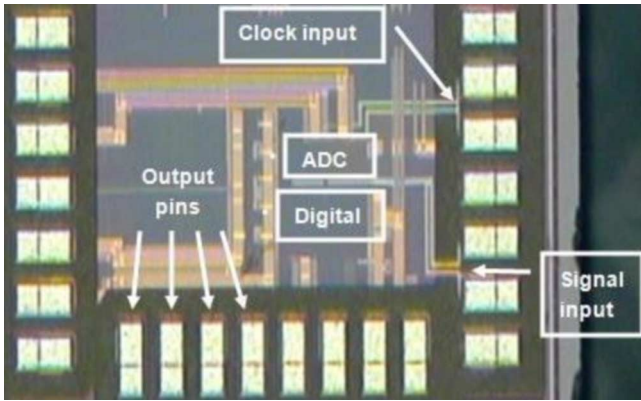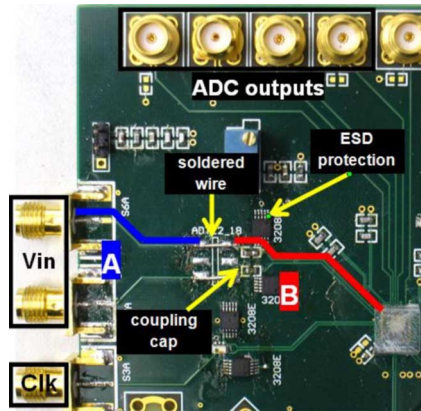
Fig. 11. Die microphotograph.

Fig. 12. PCB layout of the differential input impedance and associated discontinuities.
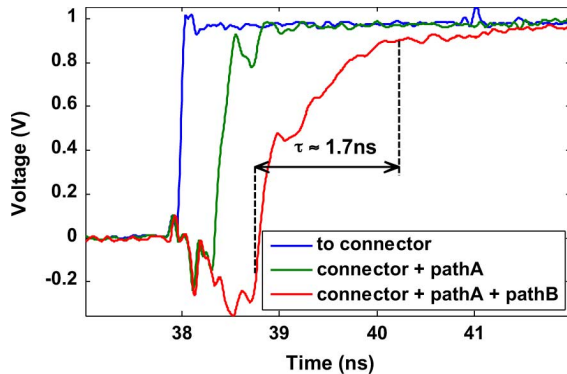

Fig. 13. Step response from a measured time-domain reflectometer at: (a) PCB input; (b) before soldered wire interface; (c) after soldered wire and ESD connection, directly to the chip input.
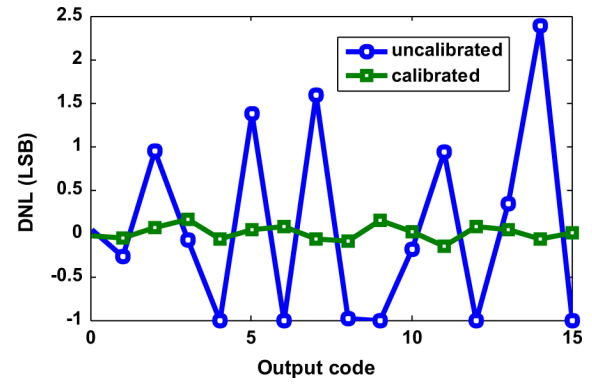

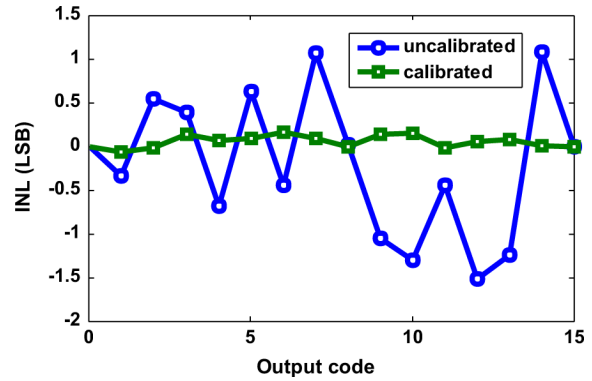Fig. 14. DNL before/after calibration.

Fig. 15. INL before/after calibration.

(a)
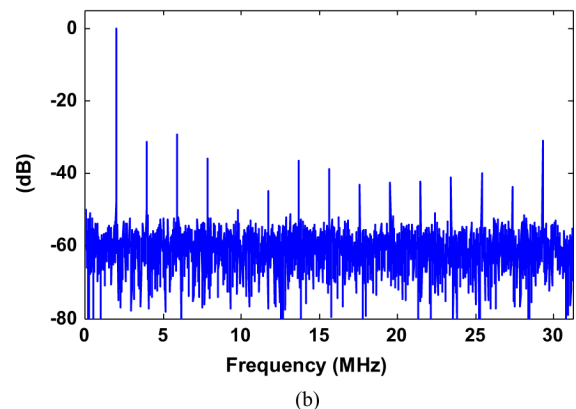
(b)

Fig. 16. Measured SNDR performance, after decimation by 64x, with f_{IN}: (a) 2.6 MHz; (b) 1.2 GHz.

before going off-chip to the logic analyzer. Before/after calibration, the measured DNL is 2.39/0.16 LSB while the INL is 1.51/0.16 LSB, respectively.

Shown in Fig. 16 is the measured ADC performance for a 2.6 MHz input, exhibiting a SNDR of 24.93 dB, and 20.72 dB with a 1.2 GHz input. Note that while the Nyquist rate after 64x decimation is 31.25 MHz, the higher frequency distortion components fold back to below this range, such that the SNDR remain unchanged after decimation.

Measured SFDR/SNDR across varying input frequencies is shown inFig. 17. At near dc (2.6 MHz), the measured ENOB is
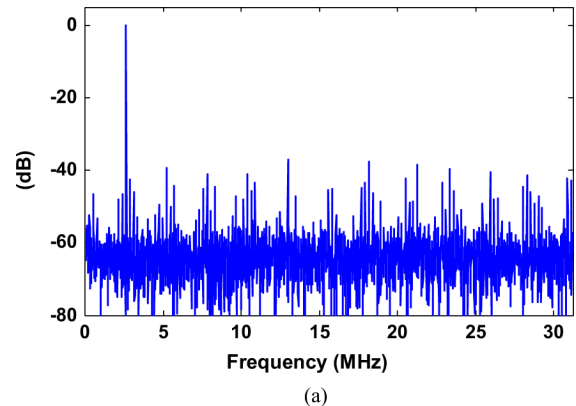
3.9b. Between 940–1500 MHz, the ENOB degrades to 3.3–3.
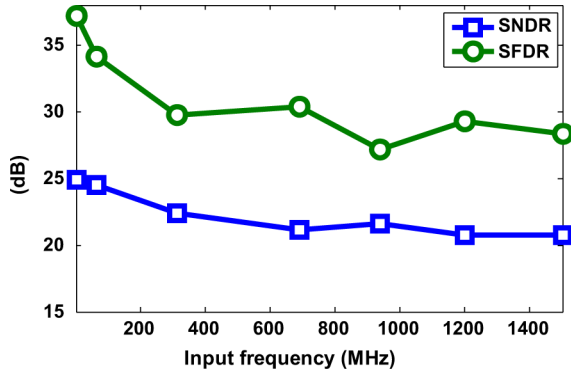
Fig. 17. SNDR/SFDR across varying input frequencies.

TABLE I
PERFORMANCE OF THE PROPOSED FLASH ADC

Process	65nm-CMOS
Resolution	4
Speed	8 Gs/s
DNL (before/after calibration)	2.39/0.16
INL (before/after calibration)	1.51/0.16
SNDR (f_{in}=2.6MHz)	24.93 dB
Supply	1V (analog) 1.2V(digital)
Input Range	0.26 V_{pp} (differential)
Power (analog)	11.2 mW
Power (CML clock buffer)	12 mW
Power (divider)	18.8 mW
Power (digital, output buffer)	24.6 mW
ERBW (Effective Resolution Bandwidth)	940 MHz
FOM ($\dfrac{P}{2^{ENOB} \cdot 2 \cdot ERBW}$)	0.86 pJ/conv.

15b, due to the input impedance discontinuities mentioned earlier.

Table I below summarizes the performance of the measured chip results.

The figure-of-merit(FoM) of this Flash ADC is compared with recent multigigahertz Flash ADCs in Fig. 18. Note that in order to normalize the power consumption relative to other works, only the analog power is factored in here, consisting of the clock buffer and comparator power. At this high sample rate, the clock power is comparable to the dynamic comparator power. The measured FoM of 0.86 pJ/conv-step compares competitively with other designs, even with the low ERBW caused by the poor input impedance matching. If we consider sampling rate instead of ERBW in the figure-of-merit, the energy consumed per conversion step is 0.2 pJ/conv-step.

VI. CONCLUSION

The effect of clock transition time for high-speed, multigigahertz T/H circuits is analyzed using a proposed signal-dependent, nonlinear model. Based on this analysis, a sine-wave sampling clock is proposed as an alternative to a traditional square-wave sampling clock for jitter-limited high-speed ADCs. As
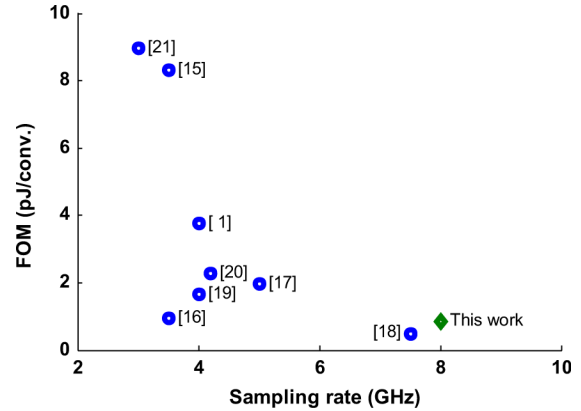

Fig. 18. Comparison of the energy-efficiency of this work versus recent multi-gigahertz Flash ADCs.

an example, an 8 Gs/s 4-bit Flash ADC in 65 nm-CMOS is built that incorporates this sine-wave sampling clock. Measurement results show that competitive energy efficiency is achievable for this sine-wave ADC when compared with conventional high-speed flash ADCs.
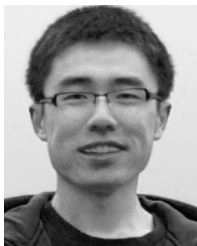
REFERENCES

[1] S. Park, Y. Palaskas, and M. Flynn, "A 4 GS/s 4b flash ADC in 0.18 μm CMOS," in *Int. Solid-State Circuits Conf. Dig.*, Feb. 2006, pp. 570–571, 674.

[2] M. Harwood *et al.*, "A 12.5 Gb/s SerDes in 65 nm CMOS using a baud-rate ADC with digital receiver equalization and clock recovery," in *Int. Solid-State Circuits Conf. Dig.*, Feb. 2007, pp. 436–437.

[3] P. Schvan *et al.*, "A 24 GS/s 6b ADC in 90 nm CMOS," in *Int. Solid-State Circuits Conf. Dig.*, Feb. 2008, pp. 544–545.

[4] K. Poulton, R. Neff, A. Muto, W. Liu, A. Burstein, and M. Heshami, "A 4 GSample/s 8b ADC in 0.35 μm CMOS," in *Int. Solid-State Circuits Conf. Dig.*, Feb. 2002, pp. 126–127.

[5] X. Jiang, Z. Wang, and M. Chang, "A 2 GS/s 6b ADC in 0.18 μm CMOS," in *Int. Solid-State Circuits Conf. Dig.*, Feb. 2003, pp. 322–323.

[6] Z. Cao, S. Yan, and Y. Li, "A 32 mW 1.25 GS/s 6b 2b/step SAR ADC in 0.13 μm CMOS," in *Int. Solid-State Circuits Conf. Dig.*, Feb. 2008, pp. 542–543.

[7] K. Poulton *et al.*, "A 20 GS/s 8b ADC with a 1 MB memory in 0.18 μm CMOS," in *Int. Solid-State Circuits Conf. Dig.*, Feb. 2003, pp. 318–319.

[8] R. H. Walden, "Analog-to-digital converter survey and analysis," *IEEE J. Sel. Areas Commun.*, vol. 17, no. 4, pp. 539–550, 1999.

[9] M. Shinagawa, Y. Akazawa, and T. Wakimoto, "Jitter analysis of high-speed sampling system," *IEEE J. Solid-State Circuits*, vol. 25, no. 1, pp. 220–224, 1990.

[10] B. Razavi, *Principles of Data Conversion System Design*. New York: IEEE Press, 1995.

[11] P. Chiang *et al.*, "A 20 Gb/s 0.13 μm CMOS serial link transmitter using an LC-PLL to directly drive the output multiplexer," in *Proc. IEEE Symp. VLSI Circuits*, 2004, pp. 272–279.

[12] P. J. Lim and B. A. Wooley, "A high-speed sample-and-hold technique using a miller hold capacitance," *IEEE J. Solid-State Circuits*, vol. 26, no. 4, pp. 643–651, 1991.

[13] M. Grozing *et al.*, "High-speed ADC building blocks in 90 nm CMOS," presented at the 4th Joint Symp. Opto- and Microelectron. Devices Circuits, Duisburg, Germany, Sep. 2006.

[14] K. Hu, T. Jiang, J. Wang, F. O'Mahony, and P. Y. Chiang, "A 0.6 mW/Gb/s, 6.4–7.2 Gb/s serial link receiver using local injection-locked ring oscillators in 90 nm CMOS," *IEEE J. Solid-State Circuits*, vol. 45, no. 4, pp. 899–908, 2010.

[15] S. Park, Y. Palaskas, A. Ravi, R. Bishop, and M. Flynn, "A 3.5 GS/s 5-b flash ADC in 90 nm CMOS," in *Proc. IEEE Custom Integr. Circuits Conf.*, 2006, pp. 489–492.

[16] K. Deguchi, N. Suwa, M. Ito, T. Kumamoto, and T. Miki, "A 6-bit 3.5-GS/s 0.9-V 98-mW flash ADC in 90 nm CMOS," in *Proc. IEEE Symp. VLSI Circuits*, 2007, pp. 64–65.

[17] M. Choi, J. Lee, J. Lee, and H. Son, "A 6-bit 5-GSample/s Nyquist A/D converter in 65 nm CMOS," in *Proc. IEEE Symp. VLSI Circuits*, 2008, pp. 16–17.

[18] H. Chung, A. Rylyakov, Z. T. Deniz, J. Bulzacchelli, G.-Y. Wei, and D. Friedman, "A 7.5-GS/s 3.8-ENOB 52-mW flash ADC with clock duty cycle control in 65 nm CMOS," in *Proc. IEEE Symp. VLSI Circuits*, 2009, pp. 268–269.

[19] Y. Lin, "A 5-bit 4.2-GS/s flash ADC in 0.13-μm CMOS," in *Proc. IEEE Custom Integr. Circuits Conf.*, 2007, pp. 213–216.

[20] S. Sheikhaei, S. Mirabbasi, and A. Ivanov, "A 43 mW single-channel 4 GS/s 4-bit flash ADC in 0.18 μm CMOS," in *Proc. IEEE Custom Integr. Circuits Conf.*, 2007, pp. 333–336.

[21] M. Kijima, K. Ito, K. Kamei, and S. Tsukamoto, "A 6b 3 GS/s flash ADC with background calibration," in *Proc. IEEE Custom Integr. Circuits Conf.*, 2009, pp. 283–286.

Feng Zhang received the B.S. degree from Beijing Institute of Technology, China, in 2000, and the M.S. and Ph.D degrees in Institute of Microelectronics of Chinese Academy of Sciences, Beijing, in 2002 and 2005, respectively.

He was an Associate Professor with institute of Microelectronics of Chinese Academy of Sciences, Beijing, and he once worked on the design of high-speed bus for the Loongson 64 bit CPU for five years from 2005 to 2010 in the Institute of Computing Technology, Chinese Academy of Sciences. In 2010, he joined the Institute of Microelectronics of the Chinese Academy of Sciences. His research interests include low-power low-jitter clock synthesis/recovery circuits (PLL and DLL) and low-power high-speed I/O links, and low-power high-speed memory design.

Zongren Yang received the B.S. degree in electrical and electronic engineering and the M.S. degree from the Microelectronics Institute, Tsinghua University, China, in 2004 and 2007, respectively.

He is an Integrated Circuit Designer at the Institute of Computing Technology, Chinese Academy of Sciences, Beijing. He worked on the development of high-speed transport.

Rui Bai was born in Chengdu, China. He received the B.S. degree in microelectronics from University of Electronic Science and Technology of China (UESTC), Chengdu, in 2008. He has been working toward the Ph.D. degree in electrical engineering at Oregon State University, Corvallis, since 2009.

His current research interests include mixed-signal and high-speed interconnection circuits.

Weiwu Hu received the Ph.D. degree in computer science from the Institute of Computing Technology, Chinese Academy of Sciences, Beijing.

He is a Professor of Computer Science at the Institute of Computing Technology. His research interests include high-performance computer architecture, parallel processing, and VLSI design.

Jingguang Wang received the B.Sc. and M.Sc. degrees in microelectronics from Fudan University, Shanghai, China, in 2003 and 2006, respectively, and the M.Sc. degree in electronic engineering from Oregon State University, Corvallis, in 2008.

From 2006 to 2007, he was an RF/Analog Design Engineer with RDA microelectronics, Shanghai, where he worked on the satellite TV tuner design. During the summer of 2008, he interned at Telegent Systems, Sunnyvale, CA, designing a SAR ADC for tuner product. In 2008, he joined Broadcom Corporation, Irvine, CA, working on the analog front-end for Ethernet products.

Patrick Chiang (S'99–M'04) received the B.S. degree in electrical engineering and computer sciences from the University of California, Berkeley, in 1998, and the M.S. and Ph.D. degrees in electrical engineering from Stanford University in 2001 and 2007.

In 1998, he was with Datapath Systems (now LSI Logic), working on analog front-ends for DSL chipsets. In 2002 he was a Research Intern at Velio Communications (now Rambus) working on 10 GHz clock synthesis architectures. In 2004 he was a consultant at startup Telegent Systems, evaluating low phase noise VCOs for CMOS mobile TV tuners. In 2006 he was a Visiting NSF Postdoctoral Researcher at Tsinghua University, China, investigating low power, low voltage RF transceivers. In 2007-2008, he was a Visiting Professor at the Institute of Computing Technology, Chinese Academy of Sciences, Beijing. In 2010, he was a Visiting Professor at the ASIC & System State Key Lab at Fudan University, China. He is currently an Assistant Professor of Electrical and Computer Engineering at Oregon State University, Corvallis. His interests include energy-efficient high-speed serial links and ADCs, impulse-based ultrawideband radios, robust near-threshold computing, and energy-constrained medical devices.

Prof. Chiang is the recipient of the 2010 Department of Energy Early CAREER award.

Lingli Xia received the B.S. degree in electronics science and technology in 2005 from Huazhong University of Science and Technology, Wuhan, China, and the Ph.D. degree in microelectronics and solid state electronics in 2010 from Fudan University, Shanghai, China.

She is currently a Postdoctor in electrical engineering at Oregon State University, Corvallis. Her doctoral thesis concerns ultra wideband RF transceiver design. Her research interests include RF front-end circuit and digital baseband circuit for wireless communication systems.